Linear Delta-f Simulations of Nonlocal Electron Heat Transport

S. Brunner,* E. Valeo, and J. A. Krommes

Princeton Plasma Physics Laboratory, P.O. Box 451, Princeton, New Jersey 08543–0451

Abstract

Nonlocal electron heat transport calculations are carried out by making use of some of the techniques developed previously for extending the δf method to transport time scale simulations [S. Brunner, E. Valeo, and J. Krommes, Phys. Plasmas **6**, 4504 (1999)]. By considering the relaxation of small amplitude temperature perturbations of an homogeneous Maxwellian background, only the linearized Fokker–Planck equation has to be solved, and direct comparisons can be made with the equivalent, nonlocal hydrodynamic approach [V. Yu. Bychenkov, W. Rozmus, V. T. Tikhonchuk, and A. V. Brantov, Phys. Rev. Lett. **75**, 4405 (1995)]. A quasineutrality-conserving algorithm is derived for computing the self-consistent electric fields driving the return currents. In the low-collisionality regime, results illustrate the importance of taking account of nonlocality in both space and time.

52.25.Fi, 52.65.Ff, 52.65.Pp

*E-mail: sbrunner@pppl.gov

I. INTRODUCTION

We report here on the progress made in extending the δf method[1–5] to transport timescale simulations. The intended, near-term application of such a scheme is the study of nonclassical drive and transport of electrons in laser–plasma interaction, eventually providing an alternative to the finite-difference approach.[6–8] Some of the general issues related to developing such a collisional δf procedure have already been addressed in reference 9:

- Evolution of the background: Over transport time scales, and under most realistic conditions, both the background f_0 and the remainder δf of the full distribution $f = f_0 + \delta f$ must be evolved simultaneously so as to maintain $\delta f / f_0 \ll 1$. This condition is necessary to preserve the advantage of the δf method over a traditional PIC approach, i.e., the reduction by a factor[1,4,5] $(\delta f / f_0)^2$ of the number of numerical particles required for lowering the sampling noise to a given level. This leads to a hybrid simulation in which the intrinsically kinetic component δf is represented with marker particles and evolved with the δf method while the parameters of the fluid component f_0, in our case a Maxwellian, are advanced with fluid equations including appropriate closure terms through δf.

- Spreading of weights in a collisional δf scheme: Besides the sampling noise common to all particle simulations, collisions turn out to be an additional, increasing source of noise in the δf approach. Indeed, unlike the collisionless case, the weights w of different markers at a particular phase space point $(\boldsymbol{x}, \boldsymbol{v})$ may take on different values in a collisional simulation. As this spreading Δw of weights increases over time, an ever increasing number of markers would be required for the simulation to be statistically resolved. A practical solution to this problem was proposed in the form of the so-called weight-spread reduction scheme.

- Sources and sinks of markers: In a collisional system, the marker particles tend to thermalize onto the background f_0, thus reducing the number of representation points at high energies where resolution might be critical. Sources and sinks of markers[10] enable a redistribution of these particles. We have carried this out by assigning each marker a finite lifetime (= sink), and immediately relocating (= source) decayed particles in the tail of the distribution.

In reference 9, a proof of principal of the above methods was given in an homogeneous plasma by computing electrical conductivity and collisional absorption. The work presented here mainly addresses issues arising for an inhomogeneous system. As a test case, we have considered the relaxation of one-dimensional temperature perturbations of a uniform, Maxwellian, electron distribution f_{M}. Conditions for nonclassical heat transport arise in the presence of temperature fluctuations having a wavelength comparable to or shorter than the effective electron mean free path, i.e., the so-called energy delocalization length (or stopping length)[11,12] $\overline{\lambda}_{\epsilon} \sim Z^{1/2}\,\overline{\lambda}_{ei}$, where $\overline{\lambda}_{ei}$ is the thermal electron–ion mean free path. In a first step, we have assumed small-amplitude perturbations, which justifies considering linearized equations in which only δf is evolved. This enabled us to focus our attention on solving for the self-consistent fields, which ensure quasineutrality in an inhomogeneous system by driving the necessary return currents as electrons tend to migrate from the hot into the cold regions. Furthermore, studying the linear regime enabled benchmarking our results against the nonlocal hydrodynamic approach by Bychenkov, Brantov *et al.*,[13–15] who derived electron transport coefficients valid in all regimes of collisionality, thus generalizing Braginskii's[16] hydrodynamic closure relations (which are limited to the Chapman–Enskog ordering). The simultaneous evolution in an inhomogeneous plasma of both components δf and f_{M}, necessary when considering large variations of the temperature profile, will be the topic of a following publication.

The remainder of this paper is organized as follows. The equations solved with the δf method are derived in Section II. For this, the limit of high ionic charge Z which leads to the "diffusive" approximation[17,7,8] of the Fokker–Planck equation is assumed. As a consequence, the $\overline{\lambda}_{ei}$ scale is not resolved, however $\overline{\lambda}_{\epsilon}$ is finite. In section III the numerical implementation is discussed, including a quasineutrality conserving algorithm for computing the self-consistent fields. Linearized δf simulations of nonclassical electron heat transport are presented in Sec. IV. Comparisons with the hydrodynamic results[13–15] illustrate the need in this second approach of taking into account not only wave number but also frequency dependence of the nonlocal transport coefficients, which leads to solving a dispersion relation for the temperature relaxation rate. Conclusions are drawn in Sec. V. A summary of the derivation of the nonlocal transport coefficients from the Fokker–Planck equation, using a generalized Laguerre polynomial representation, is given in Appendix A. Finally, a quantitative estimation of the approximation made in the δf simulations on the linearized self-collision operator[18,9] is given in Appendix B.

II. PHYSICAL MODEL

A. The effective Fokker–Planck equation in the "diffusive" approximation

The evolution of the electron distribution $f(\boldsymbol{x},\boldsymbol{v};t)$ is given by the Fokker–Planck equation

$$\frac{\partial f}{\partial t}+\boldsymbol{v}\cdot\frac{\partial f}{\partial \boldsymbol{x}}+\frac{e}{m}\frac{\partial \phi}{\partial \boldsymbol{x}}\cdot\frac{\partial f}{\partial \boldsymbol{v}}=-\left\{\,C_{ee}[f,f]+C_{ei}f\,\right\}, \tag{1}$$

where ϕ stands for the self-consistent electrostatic potential, C_{ee} stands for the Landau electron–electron self-collision operator, and C_{ei} stands for the Lorentz electron–ion collision operator. Ions are approximated as a cold, immobile, homogeneous fluid. To lighten notations, all physical quantities relative to electrons are not explicitly labeled as such, unless this is required for clarity.

Small, one-dimensional spatial perturbations of the electrons around an homogeneous Maxwellian distribution f_{M} are considered:

$$f(\boldsymbol{x},\boldsymbol{v};t)=f_{\mathrm{M}}(v)+\delta f(\boldsymbol{x},\boldsymbol{v};t), \tag{2}$$

$$f_{\mathrm{M}}(v)=\frac{N}{(2\pi v_{\mathrm{th}}^2)^{3/2}}\exp\left(-\frac{v^2}{2v_{\mathrm{th}}^2}\right), \tag{3}$$

using the definition $v_{\rm th} = (T/m)^{1/2}$ for the thermal velocity. Due to the assumption $|\delta f/f_{\rm M}| \ll 1$, we limit our attention here to solving the linearized form of Eq. (1):

$$\frac{\partial \delta f}{\partial t} + \boldsymbol{v}\boldsymbol{\cdot}\frac{\partial \delta f}{\partial \boldsymbol{x}} + \frac{e}{m}\frac{\partial \phi}{\partial \boldsymbol{x}}\boldsymbol{\cdot}\frac{\partial f_{\rm M}}{\partial \boldsymbol{v}} = -\{\widehat{C}_{ee}[\delta f] + C_{ei}\delta f\}, \tag{4}$$

where $\widehat{C}_{ee}[\delta f] = C_{ee}[f_{\rm M}, \delta f] + C_{ee}[\delta f, f_{\rm M}]$ is the linearized self-collision operator. By convention, $C_{ee}[f_{\rm M}, \delta f]$ describes scattering of δf off of the background $f_{\rm M}$, while $C_{ee}[\delta f, f_{\rm M}]$ is the reaction term that ensures conservation of momentum and energy.

The following derivation is carried out in the variables (x, v, μ), x being the direction of inhomogeneity, v being the velocity amplitude, and $\mu = v_x/v$ being the pitch angle. So as to conveniently take advantage of the additional assumption of a high ionic charge, $Z \gg 1$, a Legendre-polynomial decomposition in μ of the electron distribution is considered:

$$\delta f(x, v, \mu; t) = \sum_{l=0}^{\infty} \delta f_l(x, v; t)\, P_l(\mu). \tag{5}$$

In this representation, Eq. (4) appears in the form of an infinite set of equations for the components $\delta f_l(x, v; t)$:[19]

$$\frac{\partial\, \delta f_0}{\partial t} + \frac{v}{3}\frac{\partial\, \delta f_1}{\partial x} = -\left(\widehat{C}_{ee}[\delta f]\right)_0 \quad (l = 0), \tag{6a}$$

$$\frac{\partial\, \delta f_1}{\partial t} + v\left(\frac{\partial\, \delta f_0}{\partial x} + \frac{2}{5}\frac{\partial\, \delta f_2}{\partial x}\right) - v\frac{e}{T}\frac{\partial \phi}{\partial x}\, f_{\rm M} = -\left(\widehat{C}_{ee}[\delta f]\right)_1 - 2\,\nu_{ei}(v)\,\delta f_1 \quad (l = 1), \tag{6b}$$

$$\frac{\partial\, \delta f_l}{\partial t} + v\left(\frac{l}{2l-1}\frac{\partial\, \delta f_{l-1}}{\partial x} + \frac{l+1}{2l+3}\frac{\partial\, \delta f_{l+1}}{\partial x}\right) = -\left(\widehat{C}_{ee}[\delta f]\right)_l - l(l+1)\,\nu_{ei}(v)\,\delta f_l \quad (l \geq 2), \tag{6c}$$

with $\nu_{ei}(v) = \overline{\nu}_{ei}(v_{\rm th}/v)^3$ being the velocity dependent, and $\overline{\nu}_{ei} = e^2 N_i (Ze)^2 \ln\Lambda / 8\pi\, \epsilon_0^2\, m^2\, v_{\rm th}^3$ being the thermal e–i collision frequency. The contribution of e–e collisions to the angular harmonic equation l is noted by $(\widehat{C}_{ee}[\delta f])_l$.

Due to the assumption of large Z, $(\widehat{C}_{ee}[\delta f])_l$ can be neglected in the equations for $l \geq 1$ compared to the contribution from e-i collisions. In other words, isotropization of δf is mainly ensured by e-i collisions. However, $(\widehat{C}_{ee}[\delta f])_0$ is kept in the $l = 0$ equation, as thermalization of δf_0 by e–e collisions does not compete with e-i collisions.

Furthermore, the perturbation is assumed to vary slowly on the ν_{ei} timescale, so that the time derivatives $\partial/\partial t$ in the equations for the harmonics $l \geq 1$ can also be discarded. As shown explicitly by Eq. (A2b) of Appendix A, this leads to the neglect of electron inertia in the momentum equation.

For the δf simulations, the high-Z limit is actually taken such that $\overline{\lambda}_{ei}/\lambda_w \ll 1$, where $\overline{\lambda}_{ei} = v_{\rm th}/\overline{\nu}_{ei}$ is the thermal e-i mean free path and λ_w is a characteristic wavelength of the perturbation. As a consequence, δf remains dominantly isotropic, which enables truncating the series (5) at $l = 1$. This is the so-called "diffusive" approximation, which has often been applied in nonlinear computations.[7,8] In this ordering, however, the electron energy delocalization length (or stopping length)[11,12] $\overline{\lambda}_\epsilon = (\overline{\lambda}_{ee}\overline{\lambda}_{ei})^{1/2} = Z^{1/2}\,\overline{\lambda}_{ei}/2$, can be such that $\overline{\lambda}_\epsilon/\lambda_w \sim 1$, thus potentially giving rise to nonlocal transport. Here $\overline{\lambda}_{ee} = v_{\rm th}/\overline{\nu}_{ee}$ and $\overline{\nu}_{ee} = Ne^4 \ln\Lambda/2\pi\,\epsilon_0^2\,m^2\,v_{\rm th}^3$ are the thermal e–e mean free path and collision frequency, respectively.

From Eq.(6b) and the above discussion, it thus follows that δf_1 can be expressed as

$$\delta f_1 = -\frac{\lambda_{ei}(v)}{2}\left(\frac{\partial\,\delta f_0}{\partial x} - \frac{e}{T}\frac{\partial\phi}{\partial x}\,f_{\rm M}\right), \tag{7}$$

having defined the velocity-dependent e-i mean free path $\lambda_{ei}(v) = v/\nu_{ei}(v)$. Upon inserting (7) into (6a), one is led to an effective equation for δf_0:

$$\begin{aligned}\frac{D}{Dt}\delta f_0 \doteq \frac{\partial\,\delta f_0}{\partial t} - \frac{\partial^2}{\partial x^2}\left(\frac{v\lambda_{ei}(v)}{6}\,\delta f_0\right) + C_{ee}[f_{\rm M},\delta f_0]\\ = -\frac{v\lambda_{ei}(v)}{6}\frac{e}{T}\frac{\partial^2\phi}{\partial x^2}\,f_{\rm M} - C_{ee}[\delta f_0, f_{\rm M}],\end{aligned} \tag{8}$$

The combined effect of e-i collisions and convection has led to the second term on the left-hand side of Eq. (8), which appears as a diffusion in configuration space. The separation of the collision operator $(\widehat{C}_{ee}[\delta f])_0 = C_{ee}[f_{\rm M},\delta f_0] + C_{ee}[\delta f_0, f_{\rm M}]$ between the left- and right-hand side of Eq. (8) is done in anticipation of the numerical δf method used for solving this equation (as shown in Sec. III).

In normalized units, $\mathsf{x} = x/\lambda_w$, $\mathsf{v} = v/v_{\rm th}$, $\tau = \overline{\nu}_{ee}t$, Eq. (8) becomes:

$$\frac{\partial\,\delta f_0}{\partial\tau} - \frac{\partial^2}{\partial\mathsf{x}^2}\left[\left(\frac{\overline{\lambda}_\epsilon}{\lambda_w}\right)^2\frac{\mathsf{v}^5}{6}\,\delta f_0\right] + \frac{C_{ee}[f_{\rm M},\delta f_0]}{\overline{\nu}_{ee}} = -\left(\frac{\overline{\lambda}_\epsilon}{\lambda_w}\right)^2\frac{\mathsf{v}^5}{6}\frac{\partial^2}{\partial\mathsf{x}^2}\left(\frac{e\phi}{T}\right)f_{\rm M}(\mathsf{v}) - \frac{C_{ee}[\delta f_0, f_{\rm M}]}{\overline{\nu}_{ee}}, \tag{9}$$

clearly showing that the ratio $\overline{\lambda}_\epsilon/\lambda_w$ is the essential physical parameter of the system.

B. Quasineutrality and the equation for the self-consistent electric field

The charge displacement that would be induced by the transport of high-energy electrons down a temperature gradient must be compensated by an opposite current of cold electrons. This return current is driven by the self-consistent electric field $\boldsymbol{E} = -\partial\phi/\partial\boldsymbol{x}$.

The equation for the electrostatic potential ϕ is obtained by imposing quasineutrality. Indeed, by taking the moment $4\pi \int_0^\infty dv\, v^2$ of Eq. (6a) one obtains the linearized continuity equation:

$$\frac{\partial\, \delta N}{\partial t} + \frac{\partial\, \Gamma_x}{\partial x} = 0, \tag{10}$$

having made use of the conservation properties of the collision operator. The density perturbation and particle flux are given by

$$\delta N = \int_0^\infty dv\, (4\pi v^2)\, \delta f_0, \tag{11}$$

$$\Gamma_x = \frac{1}{3}\int_0^\infty dv\, (4\pi v^2)\; v\, \delta f_1 = -\int_0^\infty dv\, (4\pi v^2)\; \frac{v\, \lambda_{ei}(v)}{6} \left(\frac{\partial\, \delta f_0}{\partial x} - \frac{e}{T}\frac{\partial\, \phi}{\partial x}\, f_{\mathrm{M}} \right). \tag{12}$$

In (12), the contribution to the integrand proportional to δf_0 represents the flux of energetic particles down the local gradient, while the contribution proportional to ϕ describes the return currents driven by the self-consistent field.

From Eq. (10), the condition $\delta N = 0$ implies $\partial\Gamma_x/\partial x = 0$, which in turn leads to a relation for $\partial^2\phi/\partial x^2$:

$$\frac{e}{T}\frac{\partial^2\phi}{\partial x^2} = \frac{\partial^2}{\partial x^2}\left[\frac{\sqrt{2\pi}}{96} \int_0^\infty dv\, (4\pi v^2) \left(\frac{v}{v_{\mathrm{th}}}\right)^5 \delta f_0 \right], \tag{13}$$

which, according to (8), is the required quantity.

III. NUMERICAL SOLUTION

A. Solving the Fokker–Planck equation with the δf method

The δf method[1–5] is applied here to solve equation (8) for the isotropic component $\delta f_0(x, v; t)$ of the distribution perturbation. For this purpose, δf_0 is represented with a finite number n_p of so-called marker particles, each having a position x_i, velocity amplitude v_i and weight w_i:

$$\delta f_0(x, v; t) \simeq \delta \widehat{f}_0 = \frac{1}{4\pi v^2} \sum_{i=1}^{n_p} w_i(t)\, \delta\big(x - x_i(t)\big)\, \delta\big(v - v_i(t)\big). \tag{14}$$

The evolution equations for the marker particles are given by

$$\frac{dx}{dt} = \frac{\delta x_{ei}}{\delta t}, \tag{15a}$$
$$\frac{dv}{dt} = \frac{\delta v_{ee}}{\delta t}, \tag{15b}$$
$$\dot{w} \doteq \frac{dw}{dt} = -p \left(\frac{v\lambda_{ei}(v)}{6} \frac{e}{T} \frac{\partial^2 \phi}{\partial x^2} + \frac{1}{f_\mathrm{M}} C_{ee}[\delta f_0, f_\mathrm{M}] \right) + \alpha\, w, \tag{15c}$$
$$\dot{p} \doteq \frac{dp}{dt} = \alpha\, p, \tag{15d}$$

with initial conditions such that

$$w(0) = \delta f_0\big(x(0), v(0); 0\big) \,/\, g\big(x(0), v(0); 0\big), \tag{16a}$$

$$p(0) = f_\mathrm{M}\big(v(0)\big) \,/\, g\big(x(0), v(0); 0\big), \tag{16b}$$

where

$$g(x, v; t) \simeq \widehat{g} = \sum \delta\big(x - x_i(t)\big)\, \delta\big(v - v_i(t)\big) \tag{17}$$

is the marker distribution in phase space (x, v).

Let us explain point by point the content of system (15a)–(15d). This discussion will then be followed in section III B by the actual validation of these equations.

Equations (15a) and (15b), describing the evolution of markers in phase space (x, v), account for the dynamics on the left-hand side of Eq. (8). The random increments δx_{ei} and δv_{ee} over the time interval δt represent scattering in x, and e–e scattering in v off of f_M, respectively. From the spatial diffusion term in Eq. (8), one can deduce that the mean and variance of δx_{ei} must be such that

$$\frac{\langle \delta x_{ei} \rangle}{\delta t} = 0, \tag{18a}$$
$$\frac{\langle (\delta x_{ei})^2 \rangle}{2\delta t} = D_x(v) \doteq \frac{v\lambda_{ei}(v)}{6}. \tag{18b}$$

In the same way, by developing $C_{ee}[f_\mathrm{M},\delta f_0]$ in the form[19] (using again $\mathsf{v}=v/v_\mathrm{th}$)

$$C_{ee}[f_\mathrm{M},\delta f_0] = \frac{1}{v^2}\frac{\partial}{\partial v}\Big[R_v(v)\,(v^2\delta f_0) - \frac{\partial}{\partial v}D_v(v)\,(v^2\delta f_0)\Big], \tag{19a}$$

$$R_v(v) = -\overline{\nu}_{ee}v_\mathrm{th}\,\frac{1}{2\mathsf{v}^4}\Big[(1+\mathsf{v}^2)\,\mathrm{erf}(\mathsf{v}/\sqrt{2}) - \sqrt{\frac{2}{\pi}}(1+2\,\mathsf{v}^2)\,\mathsf{v}\,\exp(-\mathsf{v}^2/2)\Big], \tag{19b}$$

$$D_v(v) = \overline{\nu}_{ee}v_\mathrm{th}^2\,\frac{1}{2\mathsf{v}^3}\Big[\mathrm{erf}(\mathsf{v}/\sqrt{2}) - \sqrt{\frac{2}{\pi}}\mathsf{v}\,\exp(-\mathsf{v}^2/2)\Big], \tag{19c}$$

one obtains

$$\frac{\langle\delta v_{ee}\rangle}{\delta t} = R_v(v), \tag{20a}$$

$$\frac{\langle(\delta v_{ee})^2\rangle}{2\delta t} = D_v(v). \tag{20b}$$

The numerical implementation of Eqs. (15a)–(15b) thus requires the computation of random numbers at each time step, so that the δf scheme for a collisional system amounts to a Monte Carlo approach.

The dynamics on the right-hand side of (8) are taken into account by equation (15c) for the weight w. Actually, in (15a)–(15d) we have made use of the two-weighted δf scheme,[5] where the second weight p_i removes the statistically demanding operation of evaluating the marker distribution $g(x,v;t)$ at each time step.

To avoid computing the full integral form[19] of the reaction term $C_{ee}[\delta f_0, f_\mathrm{M}]$ at each particle position in phase space, we have made use of the simpler operator proposed by Lin *et al.*:[18]

$$C_{ee}[\delta f_0,f_\mathrm{M}]/f_\mathrm{M} \simeq \mathcal{O}[\delta f_0](x,v) = -\frac{4\sqrt{\pi}}{N\,v_\mathrm{th}^2}\,\mathcal{E}[\delta f_0](x)\,R_\epsilon(v), \tag{21a}$$

$$R_\epsilon(v) = -\frac{1}{2\mathsf{v}}\mathrm{erf}(\mathsf{v}/\sqrt{2}) + \sqrt{\frac{2}{\pi}}\,\exp(-\mathsf{v}^2/2), \tag{21b}$$

$$\mathcal{E}[\delta f_0](x) = -\int C[f_\mathrm{M},\delta f_0]\,\frac{v^2}{2}\,d\boldsymbol{v} = \overline{\nu}_{ee}v_\mathrm{th}^2\,4\pi\int_0^\infty dv\,v^2\,R_\epsilon(v)\,\delta f_0(v). \tag{21c}$$

Relation (21a)–(21c) not only ensures that the linearized collision operator $\widehat{C}\delta f \simeq C[f_\mathrm{M},\delta f] + f_\mathrm{M}\,\mathcal{O}[\delta f]$ still conserves the collisional invariants (particle number, and kinetic energy of δf_0), but also that it still annihilates a perturbed Maxwellian[18,9] of the form

$$\delta f_0 = \left[\delta N \frac{\partial}{\partial N} + \delta T \frac{\partial}{\partial T}\right] f_{\mathrm{M}} = \left[\frac{\delta N}{N} + \frac{\delta T}{T}\left(\frac{v^2}{2v_{\mathrm{th}}^2} - \frac{3}{2}\right)\right] f_{\mathrm{M}}. \tag{22}$$

A problem that arises in a collisional δf simulation is the spreading of marker weights in time[9]. Indeed, contrary to a collisionless system where there is only one possible set of values (w, p) for each position (x, v) in phase space, in a collisional system markers at the same point (x, v) take on different values. This spreading of w and p, denoted Δw and Δp respectively, is related to the fact that in the first case trajectories are deterministic, while in the second they are stochastic. As the spreads Δw and Δp tend to increase on the collision time scale, weights appear as growing additional dimensions and therefore, for a fixed number n_p of markers, are the source of increasing numerical noise. This point was discussed in detail in reference 9 where a solution to this problem was also proposed. Typically every collision time, phase space (x, v) is partitioned into a set of bins with dimensions relatively small compared to the characteristic physical lengths. Within each of these cells, a least-mean-square fit $W(x, v)$ is carried out over all marker weights w_i, which are then reassigned new values $w_i' = W(x_i, v_i)$. This results in an effective "cooling" of Δw. By considering a fit of the form

$$W(x, v) = W_0 + W_x x + W_\epsilon \frac{1}{2} v^2, \tag{23}$$

one ensures through this procedure conservation of particle number, average position, and kinetic energy of δf within each bin. A fit of the same form as (23) is also used for reducing Δp. As the system considered here is diffusive in both x and v, with average rates $(\overline{\lambda}_\epsilon/\lambda_w)^2 \overline{\nu}_{ee}$ and $\overline{\nu}_{ee}$ respectively, two sources of weight spreading are present. The frequency at which the weight-spread reduction must be carried out is therefore determined by the fastest of these rates.

Finally, in deriving the weight equations (15c) and (15d), we have made use of the possibility of adding sources and sinks of markers[10] for preserving good resolution at high velocities, where heat flux is dominant. A practical approach[9] is taken here by assigning each marker the same probability $p_\dagger = 1 - \exp(-\alpha \Delta t)$ of being annihilated at each numerical time step Δt, α being the decay rate. The terms proportional to α in (15c) and (15d) account for these deaths of neighboring particles. To conserve the total number of markers, decayed particles are immediately relocated in the tail of the distribution with zero weights (w, p). Thanks to the weight-spread reduction procedure, (w, p) then rapidly acquire new non-zero values and participate again in representing δf.

B. Validation of the marker equations

To prove that Eqs. (15a)–(15d) indeed reproduce the Fokker–Planck equation (8), one considers the distribution function F of markers in the extended phase space (x, v, w, p):[10]

$$F(x, v, w; t) \simeq \widehat{F} = \frac{1}{4\pi v^2} \sum_{i=1}^{n_p} \delta\big(x - x_i(t)\big)\, \delta\big(v - v_i(t)\big)\, \delta\big(w - w_i(t)\big)\, \delta\big(p - p_i(t)\big). \tag{24}$$

Using the equivalence between Langevin equations and the Fokker–Planck equation in the limit of high particle number, the evolution of F is described by

$$\frac{D\,F}{Dt} + \frac{\partial}{\partial w}(\dot{w}F) + \frac{\partial}{\partial p}(\dot{p}F) = -\alpha F, \tag{25}$$

where the operator D/Dt is the same as the one acting on the left-hand side of Eq. (8), and $(\dot{w}, \dot{p})$ are defined by (15c) and (15d). The corresponding initial condition is given by

$$F(x, v, w, p; 0) = g(x, v; 0)\ \delta\big(w - \delta f(x, v; 0)/g(x, v; 0)\big)\ \delta\big(p - f_{\mathrm{M}}(v)/g(x, v; 0)\big). \tag{26}$$

By taking the moments $\int dw\, dp\, w$ and $\int dw\, dp\, p$ of Eqs. (25) and (26), integrating by parts with respect to w and p (noting that F vanishes for $w, p \to \infty$), and identifying

$$\delta f_0(x, v; t) = \int F(x, v, w, p; t)\, w\, dw\, dp, \tag{27a}$$

$$f_{\mathrm{M}}(v) = \int F(x, v, w, p; t)\, p\, dw\, dp, \tag{27b}$$

it is straightforward to recover Eq. (8) for δf_0 with the correct initial condition.

C. Algorithm for computing $\partial^2\phi/\partial x^2$

To explain how the the self-consistent potential ϕ is computed simultaneously with the marker variables (x, v, w, p), we must specify more explicitly the full integration sequence that was chosen. Concerning the following notations, the superscript j of variables (x, v, w, p) indicate that they are evaluated at the integer time step $t = j\,\Delta t$. The fields $(\partial^2\phi/\partial x^2,\, \mathcal{E})$, however, are calculated at half-integer time steps $t = (j + 1/2)\,\Delta t$, and therefore carry superscript $j + 1/2$. These fields will also be assigned subscript k for their values on the spatial grid $\{x = X_k\}_{k=1,\ldots,n_x}$, which is assumed to be uniform. A full integration step over the time interval Δt therefore looks as follows:

$$\ldots \rightarrow \quad (x, v, w, p)^j \quad \xrightarrow{(\partial^2\phi/\partial x^2,\mathcal{E})^{j+1/2}} \quad (x, v, w, p)^{j+1} \quad \rightarrow \ldots \tag{28}$$

For this linear system, (x, v) can in fact be advanced independently of ϕ:

$$x_i^{j+1} = x_i^j + \delta x_{ei}(v_i^j), \tag{29a}$$

$$v_i^{j+1} = v_i^j + \delta v_{ee}(v_i^j), \tag{29b}$$

where δx_{ei} and δv_{ee} are random numbers whose statistics are given by (18a)–(18b) and (20a)–(20b), respectively. The stochastic nature of the $(x(t), v(t))$ trajectories indeed requires an explicit scheme, i.e. δx_{ei} and δv_{ee} in (29a)–(29b) can only be evaluated at v_i^j (not any predicted $v_i^{j+1/2}$, for example).

Advancing w, however, requires both fields $(\partial^2\phi/\partial x^2,\, \mathcal{E})^{j+1/2}$, as shown by the discretized form of (15c):

$$\frac{w_i^{j+1} - w_i^j}{\Delta t} = -p_i \left(\frac{v\lambda_{ei}(v)}{6} \frac{e}{T} \frac{\partial^2\phi^{j+1/2}}{\partial x^2} - \frac{4\sqrt{\pi}}{N\, v_{\mathrm{th}}^2}\, \mathcal{E}^{j+1/2}(x)\, R_\epsilon(v) \right)\Bigg|_{(x_i^{j+1/2}, v_i^{j+1/2})} . \tag{30}$$

Note that the terms in the weight equations proportional to α, which account for the decay of neighboring markers, are not considered here in the context of computing ϕ, so that in particular $p_i = \text{const}$. The whole procedure of marker sinks and sources, together with the associated correction of weights, is carried out in a separate operation and completes the full integration step over Δt.

1. First Method for Computing $\partial^2\phi/\partial x^2$

We shall now first consider the numerical implementation for ϕ that is derived directly from (13):

$$\frac{e}{T}\,\phi^{j+1/2}(x) = \frac{\sqrt{2\pi}}{96}\sum_{i=1}^{n_p} w_i^{j+1/2}\left(\frac{v_i^{j+1/2}}{v_{\rm th}}\right)^5 S(x - x_i^{j+1/2}), \tag{31}$$

S being a weighting function (or shape factor).[20] The second-order derivative of ϕ is then evaluated by finite differencing:

$$\left(\frac{\partial^2\phi}{\partial x^2}\right)_k \simeq \frac{\phi_{k+1} + \phi_{k-1} - 2\phi_k}{\Delta x^2}. \tag{32}$$

Let us also explicit the discretized form for relation (21c):[21]

$$\mathcal{E}^{j+1/2}(x) \,\simeq\, \sum_{i=1}^{n_p} w_i^{j+1/2}\,\frac{\delta(v_i^2/2)_{ee}}{\delta t}\,S(x - x_i^{j+1/2}), \tag{33}$$

where $\delta(\boldsymbol{v}_i^2/2)_{ee}/\delta t$ is the variation in time of the marker's kinetic energy due to test-particle collisions off of the background [as given by (20a)–(20b)].

Both fields $(\partial^2\phi/\partial x^2,\, \mathcal{E})$ are only computed at the finite set of grid points $\{X_k\}_{k=1,\ldots,n_x}$. When evaluating the right-hand side of equation (30) at the marker position, one then makes use of

$$\mathcal{F}(x_i) = \Delta x\sum_{k=1}^{n_x} S(X_k - x_i)\,\mathcal{F}_k, \tag{34}$$

for $\mathcal{F} = \partial^2\phi/\partial x^2,\, \mathcal{E}$. The weighting function S actually replaces the Dirac function $\delta(x - x_i)$ appearing in (14), and is the key to restricting the computation of the fields to the grid points, as shown by (31), (33), and (34).

Calculating both (31) and (33) requires $w^{j+1/2}$, estimated by

$$w^{j+1/2} = \frac{w^j \,+\, w^{j+1}}{2}. \tag{35}$$

The half-time-step values $(x, v)^{j+1/2}$ are computed in the same way.

Thus, it now appears clearly that advancing the weights w_i using (30), and computing $(\partial^2\phi/\partial x^2,\, \mathcal{E})$ through (31)–(33), must somehow be carried out simultaneously. This was attempted with an iterative method, in which first estimates $(\tilde{\phi}, \tilde{\mathcal{E}})^{j+1/2}$ for the fields were obtained by replacing $w^{j+1/2}$ by w^j into (31) and (33). These fields were then inserted into (30) for computing first approximations $\tilde{w}_i^{j+1}$ for the new weights. In a second iteration, the fields were reevaluated with $w^{j+1/2} \simeq (w^j + \tilde{w}^{j+1})/2$ and used in obtaining the final new weights w^{j+1}. This procedure for computing $(\phi, \mathcal{E})^{j+1/2}$ and w^{j+1}, as well as different refinements to it, failed in maintaining quasineutrality over many time steps. The errors related to the finite time step and finite grid size, as well as the marker sampling noise, all lead to density deviations that eventually grow to large drifts and finally to a numerical instability, as shown in Figure 1 of section IV.

In fact, the numerical relations (31) and (32) for computing $\partial^2\phi/\partial x^2$ were particularly prone to give rise to such problems. Indeed, they involve taking a second-order derivative of a high-order velocity moment of δf_0. The high moment enhances the contribution from the small fraction of highly energetic particles, reflecting their significant contribution to the flux Γ_x. This quantity is therefore all the more sensitive to marker sampling noise, and taking its second derivative further amplifies irregularities.

2. Second Method: Quasineutrality-Conserving Algorithm

The observations made with the first method for computing ϕ pointed toward the need of devising a scheme that would ensure quasineutrality exactly, taking into account all the different potential sources of numerical error. Such an algorithm can in fact be derived in a straightforward way by imposing the new weights w_i^{j+1} to leave the density δN invariant on the grid $\{X_k\}_{k=1,\dots,n_x}$ between consecutive time steps:

$$\delta N_k^{j+1} = \sum_{i=1}^{n_p} w_i^{j+1} S(X_k - x_i^{j+1}) = \sum_{i=1}^{n_p} w_i^j \, S(X_k - x_i^j) = \delta N_k^j, \qquad k = 1, \dots, n_x. \qquad (36)$$

Upon inserting Eq. (30), used for advancing the weights w_i, into Eq. (36), and making use of the interpolation relation (34), one obtains

$$\sum_{i=1}^{n_p} \left\{ w_i^j - \Delta t \, p_i \left[\frac{v\lambda_{ei}(v)}{6} \, \frac{e}{T} \, \Delta x \sum_{l=1}^{n_x} \left(\frac{\partial^2 \phi}{\partial x^2} \right)_l^{j+1/2} S(X_l - x) \right.\right.$$

$$-\frac{4\sqrt{\pi}}{N\,v_{\rm th}^2}\,\mathcal{E}^{j+1/2}(x)\,R_\epsilon(v)\Big]\Big|_{(x_i^{j+1/2},v_i^{j+1/2})}\Bigg\}\,S(X_k-x_i^{j+1})=\sum_{i=1}^{n_p}w_i^j\,S(X_k-x_i^j), \quad (37)$$

which leads to a linear system of equation for the values of $(\partial^2\phi/\partial x^2)^{j+1/2}$ on the grid:

$$\sum_{l=1}^{n_x} M_{kl}\left(\frac{\partial^2\phi}{\partial x^2}\right)_l^{j+1/2} = A_k, \qquad k=1,\dots,n_x, \tag{38a}$$

$$M_{kl}=\frac{e}{T}\sum_{i=1}^{n_p}p_i\frac{v_i^{j+1/2}\lambda_{ei}(v_i^{j+1/2})}{6}\,S(X_k-x_i^{j+1})\;\Delta x\,S(X_l-x_i^{j+1/2}), \tag{38b}$$

$$A_k=\sum_{i=1}^{n_p}\left[w_i^j\frac{S(X_k-x_i^{j+1})-S(X_k-x_i^j)}{\Delta t}+p_i\frac{4\sqrt{\pi}}{N\,v_{\rm th}^2}\,\mathcal{E}^{j+1/2}(x_i^{j+1/2})\,R_\epsilon(v_i^{j+1/2})S(X_k-x_i^{j+1})\right]. \tag{38c}$$

In (38c), $\mathcal{E}^{j+1/2}$ is again first estimated by replacing $w^{j+1/2}$ with w^j in (33), so that the linear system (38a) is defined in terms of known quantities and enables the computation of $\partial^2\phi^{j+1/2}/\partial x^2$. The new weights w_i^{j+1} are then evaluated from (30). An iteration with a new estimate for $\mathcal{E}^{j+1/2}$, obtained using an improved approximation for $w^{j+1/2}$, turned out not to be necessary. In all cases, the combination of Eqs. (30) and (38a) for computing w and ϕ self-consistently ensures that density remains unchanged on the grid to machine precision.

It can naturally be shown that the system (38a)–(38c) is equivalent to (13) in the limit of infinite marker number. In particular, the second term in relation (38c) becomes zero in this limit, reflecting conservation of particle number by the collision operator. However, for a finite number of markers, the conservation properties of the collision operator are only ensured to the precision limited by the sampling noise. The associated fluctuations are therefore taken into account in this final, quasineutrality-conserving scheme.

IV. RESULTS

A. Relaxation of sinusoidal temperature perturbations

As this study is limited to the linear regime, one needs to only consider the relaxation of sinusoidal temperature perturbations. For this purpose, the initial electron distribution $\delta f_0(x,v;t=0)$ was chosen as a perturbed Maxwellian of the form (22), with $\delta N(x,t=0)=0$ and $\delta T(x;t=0)/T=\cos(2\pi\,x/\lambda_w)$:

$$\delta f_0 = \cos(2\pi x/\lambda_w)\left(\frac{v^2}{2v_{\mathrm{th}}^2} - \frac{3}{2}\right) f_{\mathrm{M}}. \tag{39}$$

The length of the simulation box was fixed to one wavelength λ_w, and periodic boundary conditions were imposed. The evolution was then recorded by computing the temperature perturbation profile

$$\frac{\delta T(x)}{T} = \frac{1}{N}\int_0^\infty dv\,(4\pi v^2)\left(\frac{v^2}{3v_{\mathrm{th}}^2} - 1\right)\delta f_0 \simeq \frac{1}{N}\sum_{i=1}^{n_p} w_i\left(\frac{v_i^2}{3v_{\mathrm{th}}^2} - 1\right) S(x - x_i) \tag{40}$$

and its average amplitude, estimated by

$$\frac{||\delta T||}{T} = \left[\frac{2}{\lambda_w}\int_0^{\lambda_w}\left(\frac{\delta T(x)}{T}\right)^2 dx\right]^{1/2}. \tag{41}$$

The shape factor S used in diagnostic (40) is the same as for computing $(\partial^2\phi/\partial x^2,\, \mathcal{E})$. First-order (linear) weighting functions were sufficient for computing these fields. Quadratic and cubic interpolations were also tested, providing slightly smoother results.[20] The number of spatial grid points for carrying out the single-wavelength simulation was usually chosen to be $n_x = 16$.

The number of marker particles necessary for representing the two-dimensional phase space (x, v) turned out to be of the order $n_p \simeq 10^4$. The initial distribution $g(x, v)$ of marker particles was taken to be uniform in space and Maxwellian in velocity, with typical velocity spread twice the thermal velocity of the physical background f_{SM}. Good resolution was maintained by reinjecting markers at high energies ($v \sim 5v_{\mathrm{th}}$) thanks to the sources/sinks procedure applied in conjunction with the weight-spread reduction scheme.

As clearly shown by the normalized Fokker–Planck equation (9), the system contains two time scales (evaluated here at the thermal velocity): the spatial diffusion rate $\overline{\nu}_x = (\overline{\lambda}_\epsilon/\lambda_w)^2\,\overline{\nu}_{ee}$, and the e–e collision frequency $\overline{\nu}_{ee}$. The numerical time step is determined by the faster of these two rates, and is typically chosen to be $\Delta t = 10^{-2}\,\nu_{\mathrm{max}}^{-1}$, where $\nu_{\mathrm{max}} = \max(\overline{\nu}_x, \overline{\nu}_{ee})$.

Figure 1 presents the evolution in time of temperature perturbation amplitudes (41), obtained from δf simulations, having chosen the value $\overline{\lambda}_\epsilon/\lambda_w = 0.1$ for the only independent parameter of the system. This plot illustrates the problem, discussed in section III C, of computing the self-consistent electric field. Curve 1, obtained with the first method for computing $\partial^2\phi/\partial x^2$, clearly shows the onset of a numerical instability. Curve 2, however, was computed with the second algorithm, which ensures the invariance of density on the grid to machine precision. This last result presents the expected qualitative behavior: an initial transient time interval followed by an exponential relaxation until the noise level $\delta T/\delta T(0) \sim 1/n_p^{1/2}$ of the particle simulation is reached. Using an exponential fit, the relaxation rate, in this case, is estimated to be $|\nu_{\text{relax}}| = 0.29\,\overline{\nu}_{ee}$. Similar δf simulations were repeated to obtain ν_{relax} for $4\times 10^{-3} < \overline{\lambda}_\epsilon/\lambda_w < 2.5$, i.e. for approximately three orders of magnitude of the parameter $\overline{\lambda}_\epsilon/\lambda_w$. These results are plotted with circles in figure 2.

B. Comparison with the nonlocal hydrodynamic approach

A quantitative validation of our δf simulations was achieved through comparisons with the equivalent, nonlocal hydrodynamic approach presented in references 13–15. A summary of this method, together with details on its numerical solution, are given in Appendix A.

The relaxation rate for sinusoidal perturbations can be obtained from the hydrodynamic method by considering the linearized heat equation [Eq. (A2c)], Fourier-transformed with respect to space:

$$\frac{3}{2}N\frac{\partial}{\partial t}\delta T + ik\,(q_x + T\,\Gamma_x) = 0, \tag{42}$$

where the wave number is $k = 2\pi/\lambda_w$. The closure relations for the particle and heat fluxes are given by [Eqs. (A18a) and (A18b)]

$$j_x = (-e)\Gamma_x = \sigma\,E_x^\star + \alpha\,ik\,\delta T, \tag{43a}$$

$$q_x = -\alpha\,T\,E_x^\star - \chi\,ik\,\delta T, \tag{43b}$$

where the nonlocal transport coefficients (σ, χ, α), corresponding to electric conductivity , temperature conductivity, and thermoelectric conductivity, respectively, are given by Eqs.

(A20a)–(A20c). The condition of zero flux $\Gamma_x = 0$, resulting from the quasineutrality assumption, enables one to eliminate the effective electric field $E^\star_x$ from the system (42)–(43b), providing an equation for the temperature perturbation amplitude:

$$\frac{\partial}{\partial t}\delta T = -\frac{2}{3}\frac{k^2}{N}\,\chi^\star\,\delta T, \tag{44}$$

with the effective temperature conductivity being given by

$$\chi^\star = \chi - \frac{T\,\alpha^2}{\sigma}. \tag{45}$$

From (44) one thus obtains the relaxation rate:

$$\nu_{\rm relax} = -\frac{2}{3}\frac{k^2}{N}\,\chi^\star. \tag{46}$$

As a first estimate, the rate $\nu_{\rm relax}$ was evaluated for $\chi^\star = \chi^\star(k, \nu = 0)$. This basically enabled one to use the numerical values published in references 13 and 14, where the transport coefficients are given for zero frequency. Nonetheless, to be fully consistent with the δf simulations, they actually needed to be recomputed in the limit $k\overline{\lambda}_{ei} \to 0$. Taking account of effects from finite $k\overline{\lambda}_{ei}$ turns out to lead only to minor corrections ($< 10\%$, for $Z \geq 8$) for the here-considered range $\overline{\lambda}_\epsilon/\lambda_w \lesssim 10$. Finite $k\overline{\lambda}_{ei}$ naturally become important for larger values of $\overline{\lambda}_\epsilon/\lambda_w$. Neglecting the frequency dependence of the transport coefficients by only considering their value for $\nu = 0$ corresponds to discarding $\nu \sim \nu_{\rm relax}$ in Eq. (A11). Comparing the relative importance of the different terms in (A11), this approximation is justified for $\nu_{\rm relax} \ll \nu_{ee}$, $(k\,\overline{\lambda}_\epsilon)^2\nu_{ee}$. Both these conditions are violated for $\overline{\lambda}_\epsilon/\lambda_w \gtrsim 0.1$, as can be seen from figure 2, where results marked with stars represent $\nu_{\rm relax}$ obtained with $\chi^\star(k, 0)$. This explains the large deviations for $\overline{\lambda}_\epsilon/\lambda_w \gtrsim 0.1$ in Fig. 2 between this first set of hydrodynamic rates and the δf simulation results.

To derive the relaxation rate from (46), by consistently taking into account the frequency dependence of the transport coefficients $\chi^\star$, one must in fact solve the following dispersion relation for $\nu = \nu_{\rm relax}$:

$$\nu = -\frac{2}{3}\frac{k^2}{N}\,\chi^\star(k, \nu). \tag{47}$$

As will be shown in Figs. 3(e) and 3(f), this equation has more than one solution, corresponding to different modes of the system. This fact accounts for the initial transients in the δf computations, reflecting the more rapid decay of the faster damped modes. The rate derived in these simulations from the following exponential decrease of δT is therefore related to the relaxation of the slowest mode, and must be compared to the lowest rate given by Eq. (47). This solution to the dispersion relation has been obtained, for different values of $\overline{\lambda}_\epsilon/\lambda_w$, by recomputing the nonlocal transport coefficients for non-zero frequencies. This second set of hydrodynamic results has also been plotted in Fig. 2 (crosses), providing satisfactory agreement with the δf simulations.

Finally, the collisional limit for $\nu_{\rm relax}$ was derived from the classical transport coefficients for high Z:[16,13,14]

$$\nu_{\rm relax} = -(2\pi)^{3/2}\frac{128}{3}\left(\frac{\overline{\lambda}_\epsilon}{\lambda_w}\right)^2 \overline{\nu}_{ee}, \tag{48}$$

and, as a reference, has also been indicated in Fig. 2. Note that this classical limit becomes an acceptable approximation only for $\overline{\lambda}_\epsilon/\lambda_w \lesssim 10^{-2}$.

Temperature amplitude relaxation and mode spectra, in the collisional and collisionless regime, are compared in Figs. 3. Figures 3(a), 3(b), and 3(c) are related to the value $\overline{\lambda}_\epsilon/\lambda_w = 4\times 10^{-3}$, while Figs. 3(d), 3(e), and 3(f) correspond to $\overline{\lambda}_\epsilon/\lambda_w = 2.5$.

Figures 3(a) and 3(d) present the graphical solution to the dispersion relation (47). The relaxation rate $\nu_{\rm relax}$ as a function of frequency ν, given by (46), has been plotted with full curves. Their intersection with the dashed lines $\nu_{\rm relax} = \nu$ provide the solutions to the dispersion relation. These two figures illustrate that in all regimes there are many solutions to the dispersion relation for $\nu < 0$ (probably an infinity). Also, in the collisional limit, $\nu_{\rm relax}(\nu = 0)$ is clearly a good approximation for the least damped solution $\nu_{\rm solution}$ of the dispersion relation, while there is a large difference (factor ~ 10) between $\nu_{\rm relax}(\nu = 0)$ and $\nu_{\rm solution}$ for $\overline{\lambda}_\epsilon/\lambda_w = 2.5$.

In the hydrodynamic approach, the mode structure can be derived from Eqs. (A16), (A18a), and (A19) together with the constraints $\Gamma_x, \delta N = 0$:

$$\delta f_0(\nu) = \frac{1}{\nu D_{NT}^{NT} - J_T^T} \left\{ [1 - \nu\, \psi^N(\nu)] J_N^T + (\nu J_N^N - 1) \psi^T(\nu) \right\} \frac{\delta T(\nu)}{T} f_{\mathrm{M}}, \tag{49}$$

which must be evaluated for the $\nu = \nu_{\text{solution}}$ given by the dispersion relation (47). This structure, normalized with the measure $2\pi v$, is shown as a function of the energy variable $\epsilon = (1/2)(v/v_{\text{th}}^2)$ in Figs. 3(b) and 3(e) for the least damped mode. The distribution function $\delta f_0(\epsilon)$ from the particle simulation, at an arbitrary point x (here $x = \lambda_w/2$) and towards the end of the run when the transient period is over, has also been plotted in Figs. 3(b) and 3(e), and in both cases reproduces the hydrodynamic mode. Finally, note that in the collisional regime the mode structure is essentially identical to the initial perturbed Maxwellian state (39) of the δf simulation, while in the collisionless regime the same initial state is obviously the superposition of more than just the least damped mode.

The relaxation of the temperature perturbation amplitude, obtained from the δf simulation, is shown for both regimes in Figs 3(c) and 3(f). In the case $\overline{\lambda}_\epsilon/\lambda_w = 4 \times 10^{-3}$, the temperature amplitude has only relaxed by $\sim 25\%$ at the end of the transient period, while for $\overline{\lambda}_\epsilon/\lambda_w = 2.5$ the perturbation has been reduced by an order of magnitude before the system enters its asymptotic evolution. This is related to the many modes contained by the initial condition for $\overline{\lambda}_\epsilon/\lambda_w = 2.5$, as well as to the relatively small ratio between the damping rates ν_1 and ν_2 of the first and second least damped modes, respectively [$\nu_2/\nu_1 \simeq 5.5$ for $\overline{\lambda}_\epsilon/\lambda_w = 2.5$, compared to $\nu_2/\nu_1 \simeq 21$ for $\overline{\lambda}_\epsilon/\lambda_w = 4 \times 10^{-3}$, as illustrated in Figs. 3(a) and 3(b)]. Obtaining a good estimate for ν_{relax} in the low-collisional regime thus requires a relatively high number of markers to accurately resolve the asymptotic relaxation before the simulation reaches the noise level. This fact accounts for the small differences, observed in Fig. 2 for $\overline{\lambda}_\epsilon \sim \lambda_w$, between the results obtained with the δf method (circles) and the hydrodynamic approach (crosses). The remaining deviations can then essentially be explained by the approximation made on the collision operator in the δf method, as estimated in Appendix B.

V. CONCLUSIONS

The linear study of nonlocal electron heat transport has provided a useful test case in an inhomogeneous plasma to the ongoing effort of extending the δf method to transport time scale simulations. The critical issue for enabling these calculations has been the derivation of a numerically stable procedure for computing the self-consistent fields that drive the return currents. This was achieved by ensuring the numerical invariance of the electron density on the spatial grid, in particular taking into account the numerical fluctuations inherent to a particle code. By now, first nonlinear simulations have already been performed, basically using the same algorithm for computing the electric fields; this will be described in a following paper. The efficient computation of the return currents seems to represent an advantage over finite-difference codes,[22] and thus provides a further argument in favor of the δf approach as an alternative to carrying out such transport simulations.

The reduction of marker weight spreading for preventing the increase of numerical noise, and the implementation of marker sinks and sources for achieving good resolution of the small fraction of high energetic particles, have also been essential for carrying out these transport simulations.

In the linear regime considered here, we have mainly computed the relaxation of sinusoidal temperature perturbations. By comparing the δf simulation results to those obtained using the hydrodynamic approach, we have pointed out the importance in the nonclassical regime of taking account of both the wave number and the frequency dependence of the nonlocal transport coefficients. This reflects the nonlocality of transport not only in space but also in time. This point might be relevant for improving nonlocal heat-flow models based on convolution models, which to our knowledge have always been derived by relating all deviations from the Spitzer–Härm flow to space nonlocality exclusively.[11,12,23]

ACKNOWLEDGMENTS

We wish to thank V. Tikhonchuk and W. Rozmus for their advice and for providing us with their numerical results for the nonlocal transport coefficients. We are also grateful to J. Albritton and E. Williams for sharing their expert knowledge on this subject.

This work was supported by the Lawrence Livermore National Laboratory under DOE Interoffice Work Order Number B344523, by the U.S. Department of Energy Contract No. DE–AC02–76–CHO–3073, and by the Swiss National Science Foundation.

APPENDIX A: HYDRODYNAMIC APPROACH TO COMPUTING THE NONLOCAL TRANSPORT COEFFICIENTS

We shall essentially repeat here the basic derivation for obtaining the transport coefficients in the nonlocal hydrodynamic approach, as presented in references.[13–15] Our aim is to make more explicit some of the analytical steps, as well as to provide additional details on the numerical computation.

The hydrodynamic procedure consists of establishing appropriate closure relations to the fluid equations. Considering a high-Z plasma submitted to small amplitude perturbations, the linearized hydrodynamic equations can be obtained by taking the moments:

$$4\pi \int_0^\infty dv\, v^2 \,\ldots, \qquad m\frac{4\pi}{3}\int_0^\infty dv\, v^3 \,\ldots, \qquad T\,4\pi \int_0^\infty dv\, v^2 \left(\frac{v^2}{3v_{\text{th}}^2} - 1\right)\ldots, \tag{A1}$$

of Eq. (6a), Eq. (6b), and again Eq. (6a), so as to obtain the continuity, momentum and heat equation, respectively:

$$\frac{\partial}{\partial t}\delta N + \frac{\partial}{\partial x}\Gamma_x = 0, \tag{A2a}$$

$$0 = -\frac{\partial}{\partial x}\left[(-e)N\phi + T\delta N + N\delta T\right] - \frac{\partial}{\partial x}\Pi_{xx} + R_{ei,x}, \tag{A2b}$$

$$\frac{3}{2}N\frac{\partial}{\partial t}\delta T + \frac{\partial}{\partial x}\left(q_x + T\,\Gamma_x\right) = 0, \tag{A2c}$$

where we define

$$\delta N = 4\pi \int_0^\infty dv\, v^2\, \delta f_0, \tag{A3a}$$

$$\delta T = \frac{T}{N} 4\pi \int_0^\infty dv\, v^2 \left(\frac{v^2}{3v_{\rm th}^2} - 1\right) \delta f_0, \tag{A3b}$$

$$\Gamma_x = \frac{4\pi}{3} \int_0^\infty dv\, v^3\, \delta f_1, \tag{A3c}$$

$$q_x = m\, \frac{2\pi}{3} \int_0^\infty dv\, v^3 (v^2 - 5v_{\rm th}^2) \delta f_1, \tag{A3d}$$

$$\Pi_{xx} = m\, \frac{8\pi}{15} \int_0^\infty dv\, v^4\, \delta f_2, \tag{A3e}$$

$$R_{ei,x} = -m\, \frac{8\pi}{3} \int_0^\infty dv\, v^3 \nu_{ei}(v)\, \delta f_1. \tag{A3f}$$

Note that for the purpose of this paper, only potential perturbations $\boldsymbol{E} = -\partial\phi/\partial\boldsymbol{x}$, and immobile ions ($\boldsymbol{u}_i = 0$) are considered. The problem of closure consists of solving the Fokker–Planck equation for δf so as to obtain relations for the particle flux Γ_x, heat flux q_x, stress tensor Π_{xx}, and e–i drag $R_{ei,x}$ in terms of the hydrodynamical forces δN, δT, and $\boldsymbol{E}$.

Contrary to the "diffusive" model developed in section II for the δf simulations, here the high-Z assumption is only used for stating that perturbations are quasistationary and isotropization is dominated by e–i collisions, i.e., $\partial/\partial t$ and $\left(\widehat{C}_{ee}[\delta f]\right)_l$ are neglected compared to ν_{ei} for $l > 1$ in system (6a)–(6c). In particular, this led to the neglect of electron inertia in Eq. (A2b). No ordering is assumed for $\overline{\lambda}_{ei}/\lambda_w$, so that one must consider the complete set of angular harmonics δf_l of the distribution function. This nonlocal hydrodynamic approach thus encompasses the full transition from the collisional limit —recovering Braginskii's results[16] for high Z— to the fully collisionless regime.

The infinite system (6a)–(6c) can in fact again be reduced to an effective equation for δf_0:

$$\frac{\partial\, \delta f_0}{\partial t} + k^2 \frac{v\, \lambda_{ei}(v)}{6\, H_1(k\, \lambda_{ei}(v))} \left(\delta f_0 - \frac{e\phi}{T} f_{\rm M}\right) = -\widehat{C}_{ee}(\delta f_0), \tag{A4}$$

obtained by working in Fourier representation with respect to space (A being an arbitrary quantity):

$$A(k) = \int_{-\infty}^{+\infty} A(x) \exp(-ikx)\, dx, \tag{A5}$$

and thanks to the introduction of a renormalized e–i collision frequency[24] $\nu_{ei}^{\star}(k,v) = \nu_{ei}(v)H_1(k\,\lambda_{ei})$, where

$$H_l(x) = 1 + \frac{a_{l+1}}{H_{l+1}}, \tag{A6a}$$

$$a_l = \frac{x^2}{(4l^2-1)(l^2-1)}. \tag{A6b}$$

In practice, a useful and accurate approximation for H_1 is given by[24,14] $H_1(x) \simeq [1 + (\pi x/12)^2]^{1/2}$. One can easily show, by converting to normalized units, that Eq. (A4) includes both scales $k\lambda_{ei}$ and $k\lambda_\epsilon$. In the limit $k\lambda_{ei} \ll 1$, $H_1 \to 1$, and one recovers Eq. (8) from (A4).

In order to express δf_0 in terms of the forces δN, δT and ϕ, one considers the Laplace transform with respect to time:

$$A(\nu) = \int_0^\infty A(t)\exp(-\nu t)\,dt, \tag{A7}$$

so that equation (A4) becomes

$$\left(\nu + k^2\,\frac{v\lambda_{ei}(v)}{6\,H_1}\right)\left(\delta f_0(\nu) - \frac{e\,\phi(\nu)}{T} f_{\mathrm{M}}\right) = -\nu\frac{e\,\phi(\nu)}{T} f_{\mathrm{M}} - \widehat{C}_{ee}[\delta f_0] + \delta f_0(0), \tag{A8}$$

and one assumes the initial condition $\delta f_0(0)$ to be a perturbed Maxwellian of the form (22):

$$\delta f_0(0) = \left[\frac{\delta N(0)}{N} + \frac{\delta T(0)}{T}\left(\frac{v^2}{2v_{\mathrm{th}}^2} - \frac{3}{2}\right)\right] f_{\mathrm{M}}. \tag{A9}$$

As intended, the Laplace transform $\delta f_0(\nu)$ can then be expressed in the form

$$\delta f_0(\nu) = \left[\frac{e\,\phi(\nu)}{T} + \left(\frac{\delta N(0)}{N} - \nu\frac{e\,\phi(\nu)}{T}\right)\psi^N + \frac{3}{2}\frac{\delta T(0)}{T}\,\psi^T\right] f_{\mathrm{M}}, \tag{A10}$$

where the basis functions ψ^ρ ($\rho = N, T$) represent the elementary solutions to Eq. (A8):

$$\left(\nu + k^2\,\frac{v\lambda_{ei}(v)}{6\,H_1}\right)\psi^\rho + \frac{1}{f_{\mathrm{M}}}\widehat{C}_{ee}[f_{\mathrm{M}}\psi^\rho] = S_\rho, \qquad \rho = N, T, \tag{A11}$$

for the different sources S_ρ:

$$S_N = 1, \qquad S_T = \frac{v^2}{3v_{\mathrm{th}}^2} - 1. \tag{A12}$$

By taking the appropriate moments of Eq.(A10), one can express $\delta N(\nu)$ and $\delta T(\nu)$ in terms of the initial values $\delta N(0)$ and $\delta T(0)$:

$$\delta N(\nu) = \quad 4\pi\int_0^\infty dv\, v^2 \delta f_0\, S_N = N\left[\frac{e\,\phi(\nu)}{T} + \left(\frac{\delta N(0)}{N} - \nu\frac{e\,\phi(\nu)}{T}\right) J_N^N + \frac{3}{2}\frac{\delta T(0)}{T}\, J_N^T\right], \quad \text{(A13a)}$$

$$\delta T(\nu) = \frac{T}{N}4\pi\int_0^\infty dv\, v^2 \delta f_0\, S_T = T\left[\qquad\qquad \left(\frac{\delta N(0)}{N} - \nu\frac{e\,\phi(\nu)}{T}\right) J_T^N + \frac{3}{2}\frac{\delta T(0)}{T}\, J_T^T\right], \quad \text{(A13b)}$$

which can be inverted to yield

$$\frac{\delta N(0)}{N} - \nu\frac{e\,\phi(\nu)}{T} = \frac{1}{D_{NT}^{NT}}\left[\quad \left(\frac{\delta N(\nu)}{N} - \frac{e\,\phi(\nu)}{T}\right) J_T^T - \frac{\delta T(\nu)}{T} J_N^T\right], \quad \text{(A14a)}$$

$$\frac{3}{2}\frac{\delta T(0)}{T} = \frac{1}{D_{NT}^{NT}}\left[-\left(\frac{\delta N(\nu)}{N} - \frac{e\,\phi(\nu)}{T}\right) J_T^N + \frac{\delta T(\nu)}{T} J_N^N\right]. \quad \text{(A14b)}$$

In deriving relations (A13a)–(A14b), one has made use of the moments

$$J_\eta^\rho = \frac{4\pi}{N}\int_0^\infty dv\, v^2\, \psi^\rho\, f_{\mathrm{M}}\, S_\eta \quad \text{(A15)}$$

as well as the definition $D_{\eta\nu}^{\rho\delta} = J_\eta^\rho J_\nu^\delta - J_\nu^\rho J_\eta^\delta$. Furthermore, it follows from the self-adjoint property of $\widehat{C}_{ee}$ that $J_\eta^\rho = J_\rho^\eta$. Upon inserting Eqs. (A14a) and (A14b) into equation (A10), one can express $\delta f_0(\nu)$ in terms of the "instantaneous" perturbations:

$$\delta f_0(\nu) = \left[\frac{e\,\phi(\nu)}{T} + \frac{J_T^T\psi^N - J_T^N\psi^T}{D_{NT}^{NT}}\left(\frac{\delta N(\nu)}{N} - \frac{e\,\phi(\nu)}{T}\right) + \frac{J_N^N\psi^T - J_N^T\psi^N}{D_{NT}^{NT}}\frac{\delta T(\nu)}{T}\right] f_{\mathrm{M}}. \quad \text{(A16)}$$

Starting from the Fourier- (relative to space) and Laplace- (relative to time) transformed continuity (A2a) and heat (A2c) equations:

$$\nu\,\delta N(\nu) - \delta N(0) + ik\,\Gamma_x = 0, \quad \text{(A17a)}$$

$$\frac{3}{2}N\left[\nu\,\delta T(\nu) - \delta T(0)\right] + ik\left(q_x + T\,\Gamma_x\right) = 0, \quad \text{(A17b)}$$

and inserting relations (A14a)–(A14b) for $\delta N(0)$ and $\delta T(0)$, one can easily obtain the electrical current j_x and heat current q_x as a function of the generalized hydrodynamical forces:

$$j_x = (-e)\Gamma_x = \sigma\, E_x^\star + \alpha\, ik\,\delta T, \quad \text{(A18a)}$$

$$q_x = -\alpha\, T\, E_x^\star - \chi\, ik\,\delta T, \quad \text{(A18b)}$$

with the effective electric field being defined as

$$E_x^\star = -ik\left[\phi + \frac{1}{(-e)N}\left(T\,\delta N + N\,\delta T\right)\right]. \tag{A19}$$

All the quantities in (A18a)–(A18b) are naturally function of (k,ν), in particular the transport coefficients σ = electric conductivity, χ = temperature conductivity, and α = thermoelectric coefficient, given by

$$\sigma(k,\nu) = -\frac{e^2 N}{T\,k^2}\left(\nu - \frac{J_T^T}{D_{NT}^{NT}}\right), \tag{A20a}$$

$$\chi(k,\nu) = -\frac{N}{k^2}\left(\frac{5}{2}\nu - \frac{2J_T^N + J_N^N + J_T^T}{D_{NT}^{NT}}\right), \tag{A20b}$$

$$\alpha(k,\nu) = \frac{e\,N}{T\,k^2}\left(\nu - \frac{J_T^T + J_N^T}{D_{NT}^{NT}}\right). \tag{A20c}$$

It thus appears clearly that computing the transport coefficients amounts to solving equation (A11) for the different responses ψ^ρ to the sources S_ρ, from which one then obtains all moments J_η^ρ $(\eta,\rho = N,T)$ of the form (A15). The numerical solution to Eq. (A11) is obtained by considering a generalized (order 1/2) Laguerre polynomial[25] representation for ψ^ρ:

$$\psi^\rho(\epsilon) = \sum_{n=0}^{+\infty} c_n^\rho\, L_n^{(1/2)}(\epsilon), \tag{A21}$$

where $\epsilon = (1/2)\mathsf{v}^2 = (1/2)(v/v_{\rm th})^2$ is the normalized energy variable. Carrying out the projection

$$\int_0^{+\infty} d\epsilon\,\sqrt{\epsilon}\,e^{-\epsilon}\,L_n^{(1/2)}(\epsilon)\ \ldots \tag{A22}$$

onto Eq. (A11), one obtains a linear system for the coefficients c_n^ρ of decomposition (A21):

$$\sum_{m=0}^{+\infty} M_{nm}\,c_m^\rho = s_n^\rho, \qquad n = 0,1,2,\ldots \tag{A23}$$

In practice, the infinite polynomial series is truncated at $n = n_{\rm max}$, where $n_{\rm max} = 1$ is sufficient for recovering the collisional limit, and $n_{\rm max} \gtrsim 60$ in the collisionless regime is sufficient to obtain $\sim 1\%$ accuracy.

Thanks to the orthogonality relation (Γ = gamma function)[25]

$$\int_0^\infty d\epsilon\,\sqrt{\epsilon}\,e^{-\epsilon}\,L_n^{(1/2)}(\epsilon)\,L_m^{(1/2)}(\epsilon) = \frac{\Gamma(n+\frac{3}{2})}{n!}\,\delta_{n\,m}, \tag{A24}$$

the coefficients s_n^ρ in (A23) for the sources $S_N = L_0^{(1/2)}(\epsilon)$ and $S_T = -(2/3)L_1^{(1/2)}(\epsilon)$ can be written

$$s_n^N = \frac{\sqrt{\pi}}{2}\,\delta_{n\,0}, \tag{A25a}$$

$$s_n^T = -\frac{\sqrt{\pi}}{2}\,\delta_{n\,1}, \tag{A25b}$$

and the moments J_η^ρ are simply given by

$$J_\eta^\rho = \begin{cases} c_0^\rho, & \text{if } \eta = N, \\ -c_1^\rho, & \text{if } \eta = T, \end{cases} \qquad \rho = N, T. \tag{A26}$$

The detailed matrix of system (A23) appears as

$$M_{nm} = \nu\,\frac{\Gamma(n+\frac{3}{2})}{n!}\,\delta_{n\,m} + k^2\int_0^\infty d\epsilon\,\sqrt{\epsilon}\,e^{-\epsilon}\,L_n^{(1/2)}(\epsilon)\,\frac{v\,\lambda_{ei}(v)}{6\,H_1\big(k\,\lambda_{ei}(v)\big)}\,L_m^{(1/2)}(\epsilon)$$
$$+\int_0^\infty d\epsilon\,\sqrt{\epsilon}\,e^{-\epsilon}\,L_n^{(1/2)}(\epsilon)\,\frac{1}{f_{\mathrm{M}}}\widehat{C}_{ee}[f_{\mathrm{M}}L_m^{(1/2)}]. \tag{A27}$$

The first two terms on the right-hand side of (A27) are clearly symmetric. In fact, due to the self-adjoint property of the e–e self-collision operator $\widehat{C}_{ee}[\delta f_0] = C_{ee}[f_{\mathrm{M}}, \delta f_0] + C_{ee}[\delta f_0, f_{\mathrm{M}}]$, this is also the case for the last term in (A27). This can be shown explicitly by making use of[19]

$$\frac{1}{f_{\mathrm{M}}}\widehat{C}_{ee}[f_{\mathrm{M}}\psi] = -\frac{\overline{\nu}_{ee}}{\sqrt{\pi}}\,\frac{e^\epsilon}{\mathsf{v}}\,\frac{d}{d\epsilon}\left(e^{-\epsilon}G\left[\frac{d\psi}{d\epsilon}\right]\right), \tag{A28a}$$

$$G(h) = \gamma\,(3/2,\epsilon)\,h(\epsilon) - \frac{2}{3}\left[\int_0^\epsilon e^{-\epsilon'}\epsilon'^{\,3/2}h(\epsilon')\,d\epsilon' + \epsilon^{3/2}\int_\epsilon^\infty e^{-\epsilon'}h(\epsilon')\,d\epsilon'\right], \tag{A28b}$$

where $\gamma(3/2,x) = \int_0^x \sqrt{x'}\exp(-x')\,dx'$ is a generalized incomplete gamma function. The first term (multiplicative in h) on the right of relation (A28b) is related to $C_{ee}[f_{\mathrm{M}}, \delta f_0]$, while the last two (integral in h) are related to $C_{ee}[\delta f_0, f_{\mathrm{M}}]$. One can then expand:

$$\int_0^{+\infty} d\epsilon\sqrt{\epsilon}\,e^{-\epsilon}\,L_n^{(1/2)}(\epsilon)\frac{1}{f_{\mathrm{M}}}\widehat{C}_{ee}[f_{\mathrm{M}}L_m^{(1/2)}] = \frac{\overline{\nu}_{ee}}{\sqrt{2\pi}}\Big\{$$

$$
\begin{aligned}
&\int_0^{+\infty} d\epsilon\, e^{-\epsilon}\, \frac{dL_n^{(1/2)}}{d\epsilon}\, \gamma\left(3/2, \epsilon\right) \frac{dL_m^{(1/2)}}{d\epsilon} \\
&- \frac{2}{3} \int_0^{+\infty} d\epsilon\, e^{-\epsilon}\, \frac{dL_n^{(1/2)}}{d\epsilon} \int_0^{\epsilon} d\epsilon'\, e^{-\epsilon'} \epsilon'^{\,3/2}\, \frac{dL_m^{(1/2)}}{d\epsilon'} \\
&- \frac{2}{3} \int_0^{+\infty} d\epsilon\, e^{-\epsilon}\, \frac{dL_m^{(1/2)}}{d\epsilon} \int_0^{\epsilon} d\epsilon'\, e^{-\epsilon'} \epsilon'^{\,3/2}\, \frac{dL_n^{(1/2)}}{d\epsilon'} \Bigg\}, \qquad \text{(A29)}
\end{aligned}
$$

which is indeed symmetric. Thus, matrix M_{nm} of system (A23) is itself symmetric.

APPENDIX B: QUANTITATIVE ESTIMATE OF THE APPROXIMATION $\widehat{C} \simeq C[f_{\mathrm{M}}, \delta f] + f_{\mathrm{M}} \mathcal{O} \delta f$ FOR THE LINEARIZED COLLISION OPERATOR

To obtain a quantitative estimate of the approximation made in the δf simulations by replacing the reaction term $\widehat{C}_{ee}[\delta f_0, f_{\mathrm{M}}]$ with the operator $\mathcal{O}[\delta f_0] f_{\mathrm{M}}$, as defined by (21a)–(21c), we have repeated the computation of the nonlocal transport coefficients in the hydrodynamic approach with this same simplification to the e–e collision operator. To carry this out, the last two terms, related to $\widehat{C}_{ee}[\delta f_0, f_{\mathrm{M}}]$, in the contribution (A29) to the matrix M_{nm} of system (A23), must be replaced by

$$
\begin{aligned}
&\int_0^{+\infty} d\epsilon \sqrt{\epsilon}\, e^{-\epsilon}\, L_n^{(1/2)}(\epsilon)\, \mathcal{O}[f_{\mathrm{M}} L_m^{(1/2)}] \\
&\qquad = -8\, \overline{\nu}_{ee} \int_0^{+\infty} d\epsilon \sqrt{\epsilon}\, e^{-\epsilon} R_\epsilon(v)\, L_n^{(1/2)}(\epsilon) \int_0^{+\infty} d\epsilon \sqrt{\epsilon}\, e^{-\epsilon} R_\epsilon(v)\, L_m^{(1/2)}(\epsilon) \\
&\qquad = -\frac{4}{\pi}\, \overline{\nu}_{ee} \int_0^{+\infty} d\epsilon\, e^{-\epsilon}\, \frac{dL_n^{(1/2)}}{d\epsilon}\, \gamma\left(3/2, \epsilon\right) \int_0^{+\infty} d\epsilon\, e^{-\epsilon}\, \frac{dL_m^{(1/2)}}{d\epsilon}\, \gamma\left(3/2, \epsilon\right), \qquad \text{(B1)}
\end{aligned}
$$

having used

$$
R_\epsilon(v) = \frac{1}{\sqrt{2\pi}} \left[e^{-\epsilon} - \frac{1}{\sqrt{\epsilon}} \gamma\left(3/2, \epsilon\right) \right]. \qquad \text{(B2)}
$$

Contribution (B1) is still clearly symmetric.

The transport coefficients computed with the simplified collision operator were then again used for obtaining temperature relaxation rates ν_{relax} by solving the dispersion relation (47). These new results were then compared to those obtained with the full collision operator [results labeled with ($\times$) in Fig. 2], and the relative errors have been plotted in figure 4. The maximum deviation of $\sim 25\%$ occurs in the intermediate regime $\overline{\lambda}_\epsilon / \lambda_w \simeq 0.1$, where collisions are still of importance but the distribution is already significantly non-Maxwellian. This observation makes sense in view of how the model operator $\mathcal{O}[\delta f_0] f_{\mathrm{M}}$ was constructed,[18] i.e., essentially by requiring $\widehat{C} \simeq C[f_{\mathrm{M}}, \delta f] + f_{\mathrm{M}} \mathcal{O} \delta f$ to conserve the collision invariants and to annihilate the correct equilibrium states, however without imposing any condition so as to guarantee the accurate relaxation rate in energy of a non-Maxwellian distribution.

REFERENCES

[1] M. Kotschenreuther, Bull. Am. Phys. Soc. **34**, 2107 (1988).

[2] M. Kotschenreuther, in *Proceedings of the 14th International Conference on the Numerical Simulation of Plasmas*, Annapolis, MD, September 1991 (APS, College Park, MD, 1991), Paper PT20.

[3] S. E. Parker and W. W. Lee, Phys. Fluids B **5**, 77 (1993).

[4] A. Y. Aydemir, Phys. Plasmas **1**, 822 (1994).

[5] G. Hu and J. A. Krommes, Phys. Plasmas **1**, 863 (1994).

[6] J. P. Matte and J. Virmont, Phys. Rev. Lett. **49**, 1936 (1982).

[7] J. R. Albritton, Phys. Rev. Lett. **50**, 2078 (1983).

[8] E. M. Epperlein, Laser and Particle Beams **12**, 257 (1994).

[9] S. Brunner, E. Valeo, and J. A. Krommes, Phys. Plasmas **6**, 4504 (1999).

[10] Y. Chen and R. B. White, Phys. Plasmas **4**, 3591 (1997).

[11] J. F. Luciani, P. Mora, and J. Virmont, Phys. Rev. Lett. **51**, 1664 (1983).

[12] J. R. Albritton, E. A. Williams, I. B. Bernstein, and K. P. Swartz, Phys. Rev. Lett. **57**, 1887 (1986).

[13] V. Yu. Bychenkov, W. Rozmus, V. T. Tikhonchuk, and A. V. Brantov, Phys. Rev. Lett. **75**, 4405 (1995).

[14] A. V. Brantov, V. Yu. Bychenkov, V. T. Tikhonchuk, JETP **83**, 716 (1996).

[15] A. V. Brantov, V. Yu. Bychenkov, V. T. Tikhonchuk, and W. Rozmus, Phys. Plasmas **5**, 2742 (1998).

[16] S. I. Braginskii, in *Reviews of Plasma Physics* (Consultants Bureau, New York, 1965),

Vol. 1.

[17] I. B. Bernstein, Phys. Fluids **20**, 577 (1976).

[18] Z. Lin, W. M. Tang, and W. W. Lee, Phys. Plasmas **2**, 2975 (1995).

[19] I. P. Shkarofsky, T. W. Johnston, and M. A. Bachynsky, *The Particle Kinetics of Plasmas* (Addison-Wesley, London, 1966).

[20] C. K. Birdsall and A. B. Langdon, *Plasma Physics via Computer Simulations* (Institute of Physics Publishing, Bristol, 1991).

[21] A. M. Dimits and B. I. Cohen, Phys. Rev. E **49**, 709 (1994).

[22] J. R. Albritton, private communications.

[23] E. M. Epperlein and R. W. Short, Phys. Fluids B **3**, 3092 (1991).

[24] E. M. Epperlein, R. W. Short, and A. Simon, Phys. Rev. Lett. **69**, 1765 (1992).

[25] M. Abramowitz, and I. A. Stegun, *Handbook of Mathematical Functions* (Wiley, New York, 1964).

FIGURES

FIG. 1. Evolution of temperature amplitude δT over time, for the ratio $\overline{\lambda}_\epsilon/\lambda_w = 0.1$ of the stopping length $\overline{\lambda}_\epsilon$ over the wavelength λ_w. Using method 1 for computing the self-consistent electric fields leads to a numerical instability. The expected exponential decay of the perturbation is observed with method 2, which ensures invariance of density on the spatial grid. The numerical noise level is reached for $\delta T/\delta T(0) = 1/n_p^{1/2}$; here $n_p = 10^4$.

FIG. 2. Relaxation rate $\nu_{\rm relax}$ in units of $\overline{\nu}_{ee}$ for different ratios $\overline{\lambda}_\epsilon/\lambda_w$. Results obtained with the nonlocal hydrodynamic approach using the transport coefficients at zero frequency ($\star$) clearly disagree with the δf simulations ($\circ$) at low collisionality ($\overline{\lambda}_\epsilon/\lambda_w \stackrel{\sim}{>} 0.1$). Good agreement is achieved with a second set of hydrodynamic results ($\times$), obtained by solving a dispersion relation for $\nu_{\rm relax}$ so as to take account of the frequency dependence of the transport coefficients. The classical limit (dashed line) only becomes an acceptable approximation for $\overline{\lambda}_\epsilon/\lambda_w \stackrel{\sim}{<} 10^{-2}$.

FIG. 3. Comparing results in the collisional [$\overline{\lambda}_\epsilon/\lambda_w = 4 \times 10^{-3}$, Figs. (a), (b), (c)] and collisionless [$\overline{\lambda}_\epsilon/\lambda_w = 2.5$, Figs. (d), (e), (f)] regime. The graphical solution to the dispersion relation in the nonlocal hydrodynamic approach is shown in (a) and (d). The initial (dash-dotted line) and final ($\circ$) state of the δf simulation, as well as the mode structure (full line) of the least damped mode obtained from the hydrodynamic method are given in (b) and (e). The relaxation in time of the temperature perturbation amplitude given by the δf simulation is presented in (c) and (f).

FIG. 4. Relative difference for different collisionalities between the solution $\nu_{\rm relax}$ to the dispersion relation obtained by considering the full operator $\widehat{C}_{ee}[\delta f_0, f_{\rm M}]$ [results labeled with ($\times$) in Fig. 2] and the solution obtained with the approximation $\mathcal{O}[\delta f_0] f_{\rm M}$.

FIG.1 Brunner

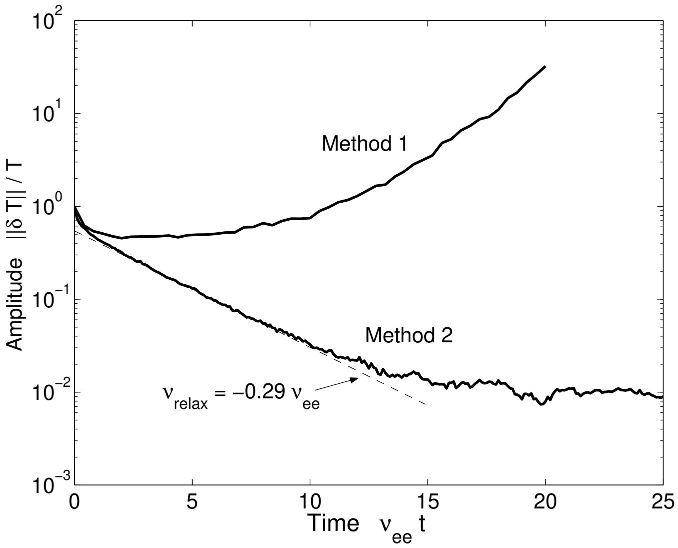

FIG.2 Brunner

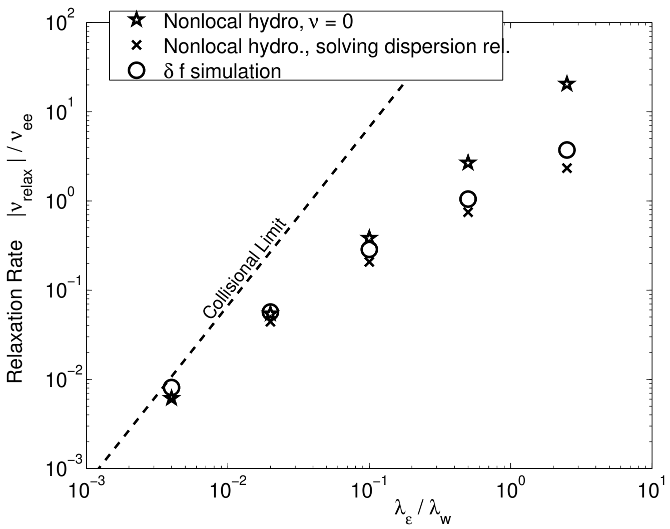

FIG.3 Brunner

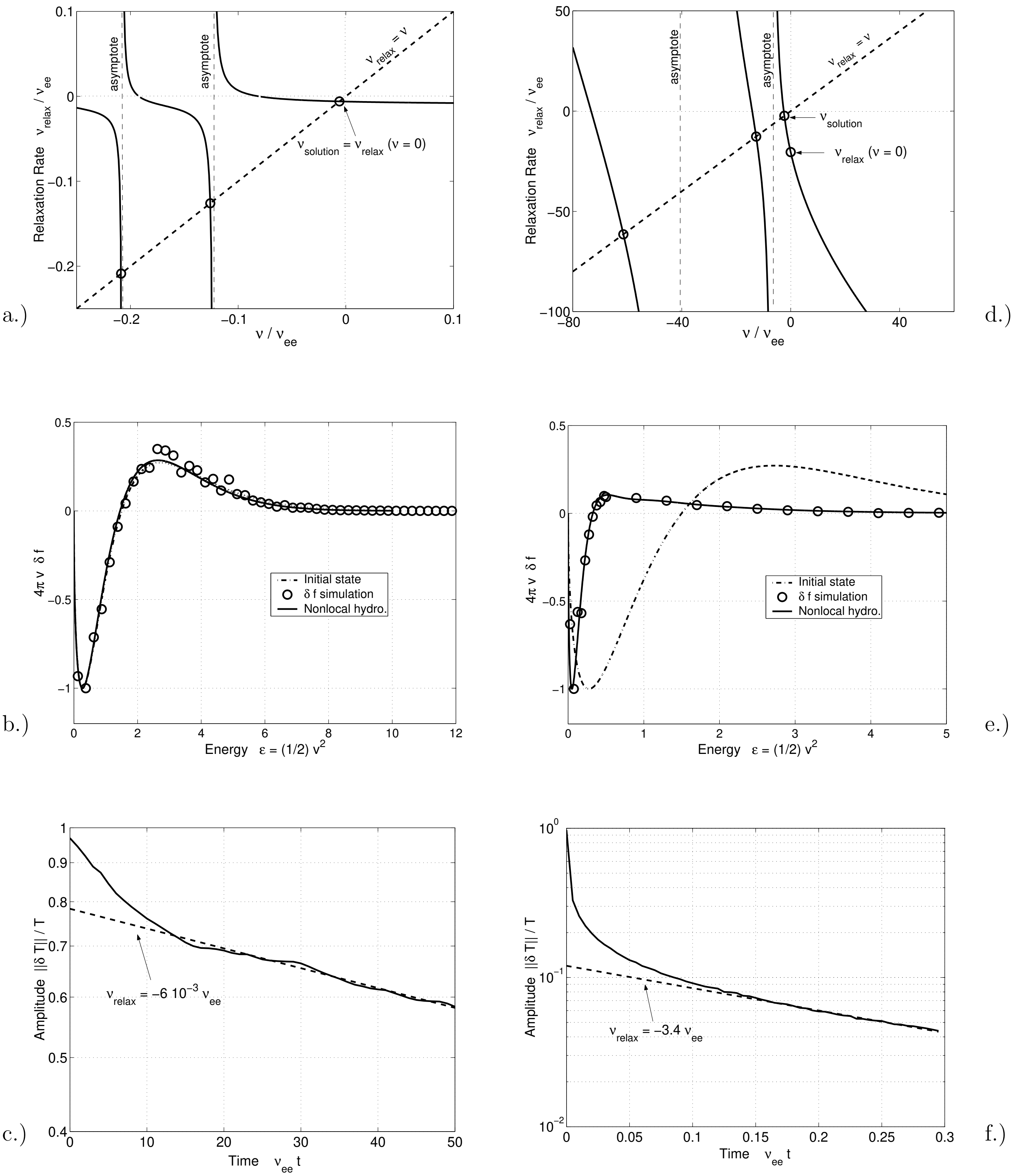

FIG.4 Brunner